Marine Structures 24 (2011) 319–337

Contents lists available at ScienceDirect

Marine Structures

journal homepage: www.elsevier.com/locate/marstruc

Nonlinear analysis of short concrete-filled double skin tube columns subjected to axial compressive forces

Hsuan-Teh Hu*, Feng-Chien Su

Department of Civil Engineering and Sustainable Environment Research Center, National Cheng Kung University, Tainan, Taiwan 701, ROC

ARTICLE INFO

Article history:
Received 25 August 2010
Received in revised form 10 March 2011
Accepted 11 May 2011

Keywords:
Concrete-filled double skin tube
Lateral confining pressure

ABSTRACT

Proper material constitutive models for concrete-filled double skin tube (CFDST) columns with circular cross-section and subjected to axial compressive forces are proposed and verified against experiment data using the nonlinear finite element program Abaqus. It is shown that CFDST columns can provide a good confining effect for concrete core, especially when the diameter-to-thickness ratios of both the outer and the inner tubes are small. In addition, empirical equations are proposed to predict the lateral confining pressure of the concrete core for CFDST columns. Finally, the axial strengths of the CFDST columns calculated by the proposed formulations are compared with AISC formulations against the experimental data. It has been shown that the proposed formulations are better than the AISC formulations.

1. Introduction

A concrete-filled tube (CFT) column consists of a steel tube filled with concrete. The steel tube acts as longitudinal and transverse reinforcement and the concrete delays the local buckling of tube. Due to the benefit of composite action of both materials, the CFT columns provide excellent seismic-resistant structural properties such as high strength, high ductility and large energy absorption capacity. Therefore, CFT columns have gained popularity in supporting heavy loads in high-rise buildings, bridges, offshore structures and marine structures. Various experimental and analytical studies have been performed on CFT columns [1–10].

* Corresponding author. Tel.: +886 6 2757575x63168; fax: +886 6 2358542.
E-mail address: hthu@mail.ncku.edu.tw (H.-T. Hu).

0951-8339/$ – see front matter © 2011 Elsevier Ltd. All rights reserved.
doi:10.1016/j.marstruc.2011.05.001

A concrete-filled double skin tube (CFDST) column with circular cross-section (Fig. 1) consists of two concentric steel tubes with concrete filled between the two tubes. The CFDST columns also have excellent resistance to seismic [11–15] and are lighter and have more fire resistant than CFT columns [16]. The ultimate strength of a CFDST column is affected by the compressive strength of the concrete, the concrete confined pressure, the yield strength of the tubes, and the diameter-to-thickness ratios of the inner and outer tubes. It is known that the circular cross-sections have the best confinement effect [8] and offshore loading resistance [17,18]. Therefore, CFDST columns with circular cross-section and subjected to axial compressive forces are studied. In this paper, the material constitutive models for concrete and steel are proposed. Then nonlinear analyses are carried out using the finite element program Abaqus [19] and verified against experiment data reported by Tao et al. [13] and Zhao et al. [15]. Finally, the effects of the outer-diameter-to-outer-thickness ratio (D_o/t_o) and the inner-diameter-to-inner-thickness ratio (D_i/t_i) on the confined pressure are studied and discussed.

2. Material properties and constitutive models

The cross-section of CFDST columns is circular, as shown in Fig. 1. The material constitutive models are given below.

2.1. Steel tube

In the numerical analysis, the Poisson's ratio ν_s of the steel tube is assumed to be 0.3. For the specimens of Tao et al. [13], the elastic modulus E_s of the steel tubes is assumed to be 200 GPa. For the specimens of Zhao et al. [15], the elastic modulus E_s is directly obtained from the experimental data. The steel tubes are simulated using an elastic-perfectly plastic model. When the steel tube is subjected to multiple stresses, a von Mises yield criterion F is employed to define the elastic limit,

$$F = \sqrt{3J_2} = \frac{1}{\sqrt{2}}\sqrt{(\sigma_1-\sigma_2)^2+(\sigma_2-\sigma_3)^2+(\sigma_3-\sigma_1)^2} = f_y \tag{1}$$

where J_2 is the second stress invariant of the stress deviator tensor, σ_1, σ_2, and σ_3 are the principal stresses, and f_y is the yield stress of the steel tube. Fig. 2 shows the von Mises yield surface in the three-dimensional principal stress space. The steel tubes behave linearly elastic when the stress points fall inside the yield surface. When stress points reach the yield surface, the steel tubes behave perfectly plastic and can not resist further loading.

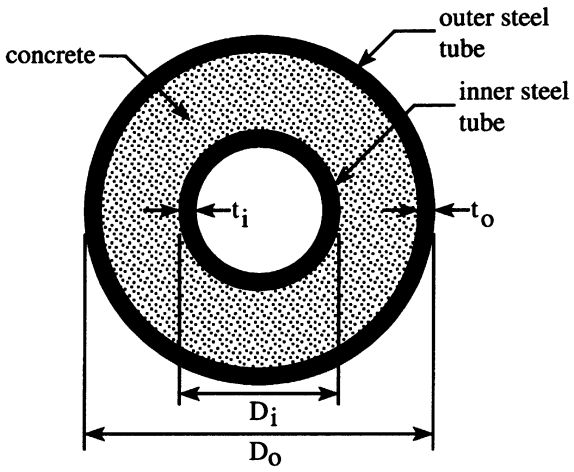

Fig. 1. Cross-section of CFDST columns.

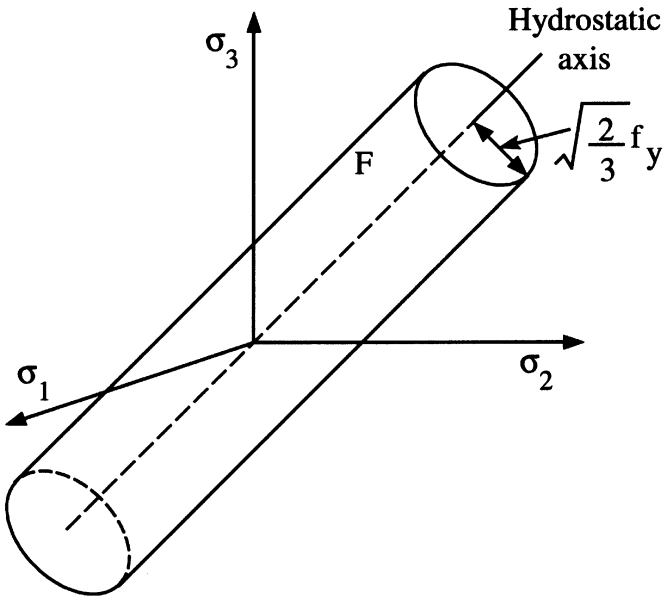

Fig. 2. von Mises yield surface in the three-dimensional principal stress space.

2.2. Concrete

The Poisson's ratio ν_c of concrete under uniaxial compressive stress ranges from 0.15 to 0.22, with a representative value of 0.19 or 0.20 [20]. In this study, the Poisson's ratio of concrete is assumed to be 0.2.

Let the uniaxial compressive strength and the corresponding strain of the unconfined concrete be f_c' and ϵ_c' (Fig. 3). The value of ϵ_c' is usually around the range of 0.002–0.003. A representative value 0.002 is used in the analysis. When concrete is subjected to laterally confining pressure, the uniaxial compressive strength f_{cc}' and the corresponding strain ϵ_{cc}' (Fig. 3) are much higher than those of unconfined concrete. The relations between f_{cc}', f_c' and between ϵ_{cc}', ϵ_c' are estimated by the following equations [21]:

$$f'_{cc} = f'_c + k_1 f_l \tag{2}$$

$$\epsilon'_{cc} = \epsilon'_c \left(1 + k_2 \frac{f_l}{f'_c}\right) \tag{3}$$

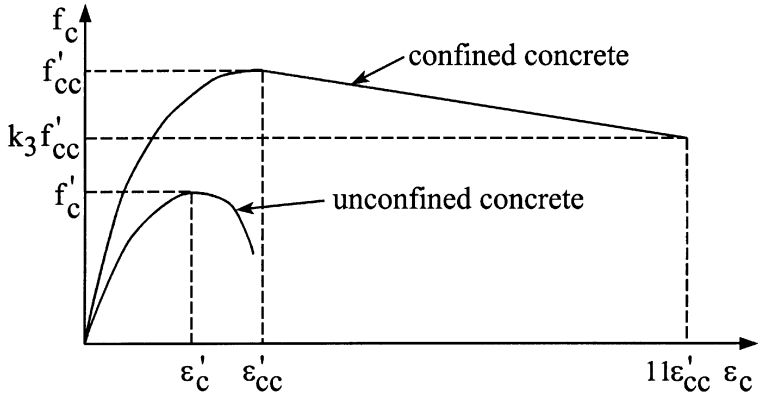

Fig. 3. Equivalent uniaxial stress–strain curve for concrete.

where f_l represents the confining pressure around the concrete core. The coefficients k_1 and k_2 are constants and can be obtained from experimental data. Meanwhile, the coefficients k_1 and k_1 are set to 4.1 and 20.5 based on the studies of Richart et al. [22].

The concrete in the CFDST columns is subjected to triaxial compressive stresses and the failure of concrete is dominated by a compressive failure surface expanding with the increasing of hydrostatic pressure. Hence, a linear Drucker-Prager yield criterion G (Fig. 4) is used to model the yield surface of concrete, which is expressed as

$$G = t - p\tan\beta - d = 0 \tag{4}$$

where

$$p = -(\sigma_1 + \sigma_2 + \sigma_3)/3 \tag{5a}$$

$$d = \left(1 - \frac{\tan\beta}{3}\right) f'_{cc} \tag{5b}$$

$$t = \frac{\sqrt{3J_2}}{2}\left[1 + \frac{1}{K} - \left(1 - \frac{1}{K}\right)\left(\frac{r}{\sqrt{3J_2}}\right)^3\right] \tag{5c}$$

$$r = \left[\frac{9}{2}\left(S_1^3 + S_2^3 + S_3^3\right)\right]^{1/3} \tag{5d}$$

and S_1, S_2, and S_3 are principal stress deviators. The constants K and β are material parameters determined from experimental data. In the analysis, K and β are set to 0.8 and 20°, respectively [8,9].

The response of the concrete is modeled using elastic-hardening plastic theory with the isotropic hardening rule and the associated flow rule. The stress–strain relationship proposed by Saenz [23] has been widely adopted as the uniaxial stress–strain curve for concrete. It has the following form:

$$f_c = \frac{E_c\epsilon_c}{1 + (R + R_E - 2)\left(\frac{\epsilon_c}{\epsilon'_{cc}}\right) - (2R - 1)\left(\frac{\epsilon_c}{\epsilon'_{cc}}\right)^2 + R\left(\frac{\epsilon_c}{\epsilon'_{cc}}\right)^3} \tag{6}$$

where

$$R = \frac{R_E(R_\sigma - 1)}{(R_\epsilon - 1)^2} - \frac{1}{R_\epsilon},\ R_E = \frac{E_c\epsilon'_{cc}}{f'_{cc}}$$

and $R_\sigma = 4, R_\epsilon = 4$ may be used [24]. The initial modulus of elasticity of concrete E_c is highly correlated to its compressive strength and can be calculated with reasonable accuracy from the empirical equation [25]:

$$E_c = 4700\sqrt{f'_{cc}}\ MPa \tag{7}$$

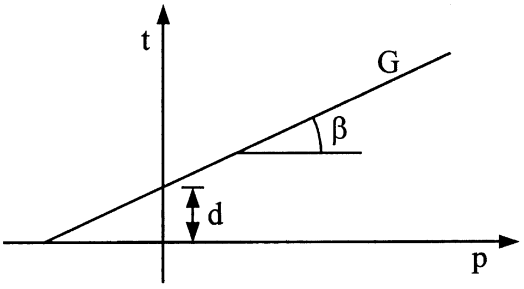

Fig. 4. Linear Drucker-Prager yield criterion for concrete.

In the analysis, Eq. (6) is taken as the equivalent uniaxial stress–strain curve for concrete when the concrete strain ϵ_c is less than ϵ_{cc}' (Fig. 3). When $\epsilon_c > \epsilon_{cc}'$, a linear descending line is used to model the softening behavior of concrete. If k_3 is defined as the material degradation parameter, the descending line is assumed to be terminated at the point where $f_c = k_3 f_{cc}'$ and $\epsilon_c = 11\epsilon_{cc}'$ [8,9].

Generally, the parameters f_l and k_3 should be provided in order to completely define the equivalent uniaxial stress–strain relationship. These two parameters depend on the diameter-to-thickness ratios D_o/t_o and D_i/t_i. Consequently, their values are determined by matching the numerical results with experimental data via parametric studies.

3. Finite element model for CFDST columns

Due to symmetry, only one-half of the CFDST columns are analyzed and a typical finite element mesh is shown in Fig. 5. Symmetry boundary conditions are enforced on the symmetric planes, which are $u = 0$ on the plane normal to the x-axis. The bottom surface of CFDST columns is assumed to be fixed with $u = v = w = 0$. The uniformly compressive loading is applied to the top surface of the column in the z direction directly. In the finite element mesh, both the concrete and the steel tubes are modeled by a 20-node solid element (three degrees of displacement freedom per node) with reduced integration rule.

There are two interfaces existed in the finite element mesh, which are the concrete to the inner tube interface and the concrete to the outer steel tube interface. Both of the interfaces are modeled by pairs of contact surfaces. The nodes on these interfaces are connected through the contact surfaces which can model infinitesimal sliding and friction [19] between the concrete and the steel tubes. The friction coefficient used in all the analyses is $\mu_s = 0.25$ [8,9]. As the results, the nodes on the interfaces are allowed to either contact or separate but not to penetrate each other.

Convergent studies of the finite element meshes have been done by the authors using various element sizes for CFDST columns. It has been shown that the numerical results are not too sensitive to the element sizes and mesh refinements. This trend is similar to that of the CFT columns [8,9].

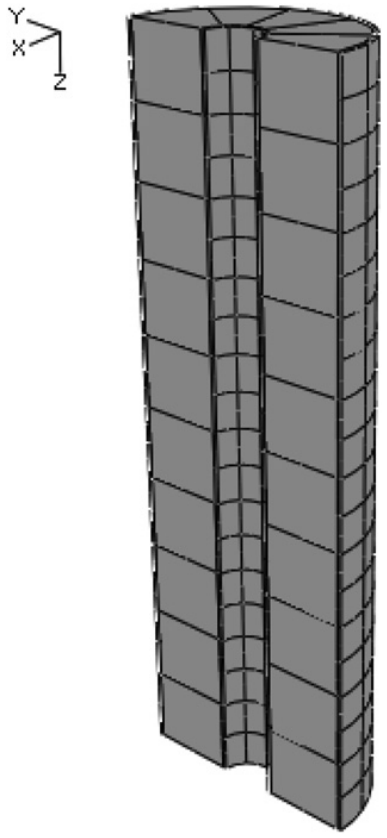

Fig. 5. Finite element mesh for CFDST columns.

4. Numerical analysis

In this section, 5 specimens from the experiment of Tao et al. [13], i.e. CC2a, CC3a, CC5a, CC6a and CC7a (Table 1) and 6 specimens from the experiment of Zhao et al. [15], i.e. C1C7, C2C7, C3C7, C4C7, C5C8 and C6C8, are used to verify and calibrate the proposed material models for the CFDST columns. For the specimens of Tao et al., the diameter-to-thickness ratios of the outer tube (D_o/t_o) and of the inner tube (D_i/t_i) range from 60 to 100 and from 16 to 55, respectively. For the specimens of Zhao et al., the diameter-to-thickness ratios of the outer tube (D_o/t_o) and of the inner tube (D_i/t_i) range from 19 to 57 and from 17 to 33, respectively. The dimensions and material properties of those CFDST columns in analyses are all given in Table 1.

4.1. Simulation of CFDST columns

Figs. 6 and 7 show the axial loading versus axial strain relations of the specimens tested by Tao et al. [13] and Zhao et al. [15]. The results of numerical simulations for the CFDST columns are given in Table 2. Generally, the numerical results show good agreements with the experiment data.

Typical failure patterns of those CFDST columns in experiments were local (outward folding) failure mechanisms as shown by the photos in Fig. 8. This is the same as that observed by many other researchers both in CFT specimens and CFDST specimens, such as Hu et al. [8], Uy [26], Zhao and Grzebieta [27]. The deformation shapes for the simulated CFDST columns close to the failure stages are shown in Figs. 9 and 10. It can be seen that the simulated failure mechanisms of the CFDST columns exhibit similar local buckling modes as those in experiments.

4.2. Parameter study for f_l

From Tables 1 and 2, it can be observed that when the diameter-to-thickness ratio of the outer tube D_o/t_o is held constant, both the ultimate strength and the lateral confining pressure f_l decrease with the

Table 1
Dimensions and material properties of CFDST columns.

Column number	D_o (mm)	t_o (mm)	D_o/t_o	D_i (mm)	t_i (mm)	D_i/t_i	Length (mm)	Yield stress f_y (MPa)		Concrete f_c' (MPa)	Tested by
								Outer tube	Inner tube		
CC2a	180	3	60	48	3	16	540	275.9	396.1	40	Tao et al.
CC3a	180	3	60	88	3	29.33	540	275.9	370.2	40	Tao et al.
CC5a	114	3	38	58	3	19.33	342	294	374	40	Tao et al.
CC6a	240	3	80	114	3	38	720	275.9	294.5	40	Tao et al.
CC7a	300	3	100	165	3	55	900	275.9	320.5	40	Tao et al.
C1C7	114.5	5.9	19.41	48.4	2.8	17.29	400	454	425	63.4	Zhao et al.
C2C7	114.6	4.7	24.38	48.4	2.8	17.29	400	416	425	63.4	Zhao et al.
C3C7	114.4	3.5	32.68	48.4	2.8	17.29	400	453	425	63.4	Zhao et al.
C4C7	114.2	3.0	38.07	48.4	2.8	17.29	400	430	425	63.4	Zhao et al.
C5C8	165.1	3.5	47.17	101.8	3.1	32.84	400	433	410	63.4	Zhao et al.
C6C8	165.3	2.9	57	101.8	3.1	32.84	400	395	410	63.4	Zhao et al.

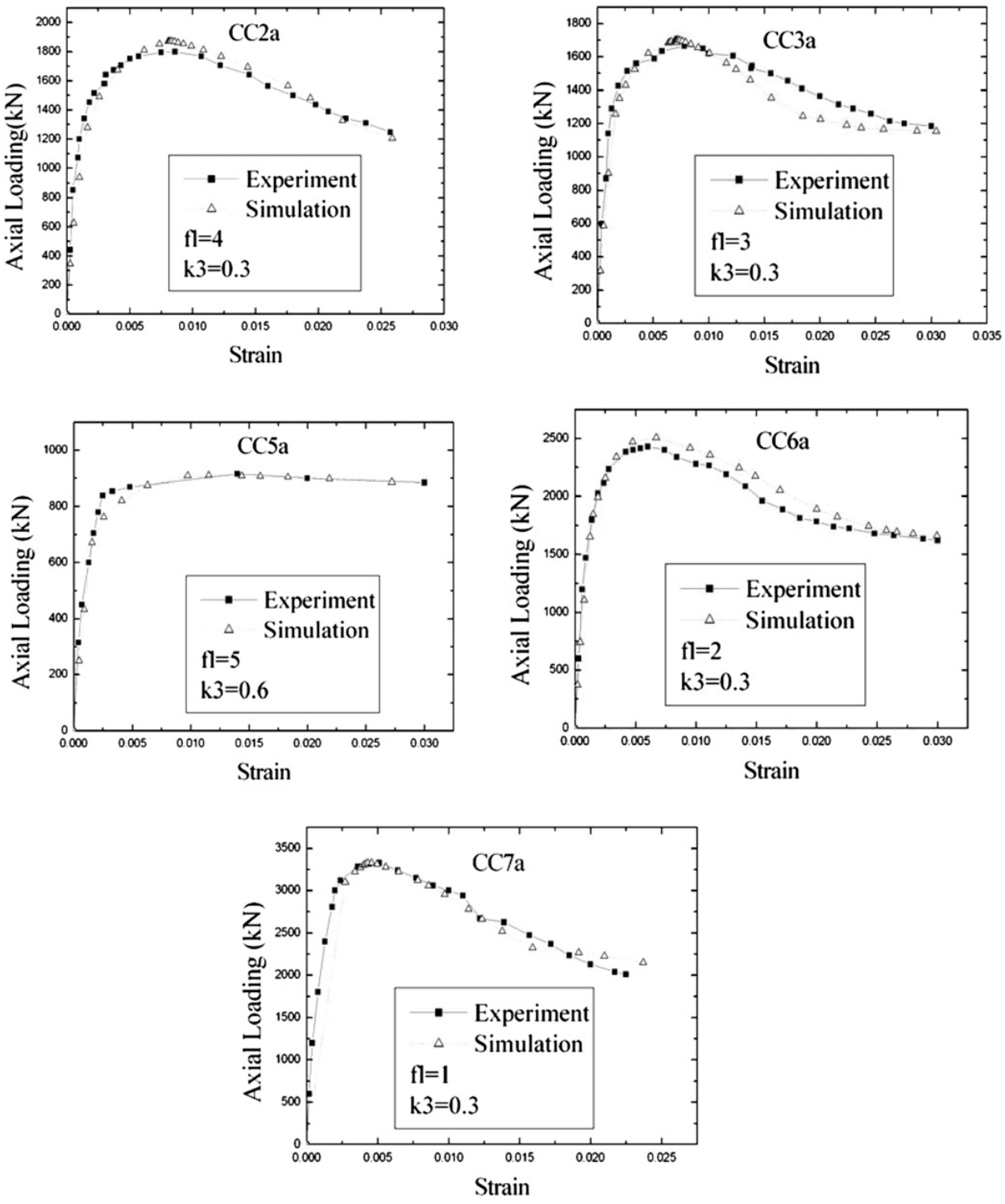

Fig. 6. Axial loading–strain relations of the CFDST columns tested by Tao et al.

increasing of the diameter-to-thickness ratio of the inner tube D_i/t_i. Similarly, when the diameter-to-thickness ratio of the inner tube D_i/t_i is held constant, both the ultimate strength and the lateral confining pressure f_l also decreases with the increasing of the diameter-to-thickness ratio of the inner tube D_o/t_o. As a result, when the D_o/t_o and the D_i/t_i ratios are small, the lateral confining pressure f_l usually has a large value (say 5 MPa for the C1C7 column) and the steel tubes provide strong lateral support to the concrete core.

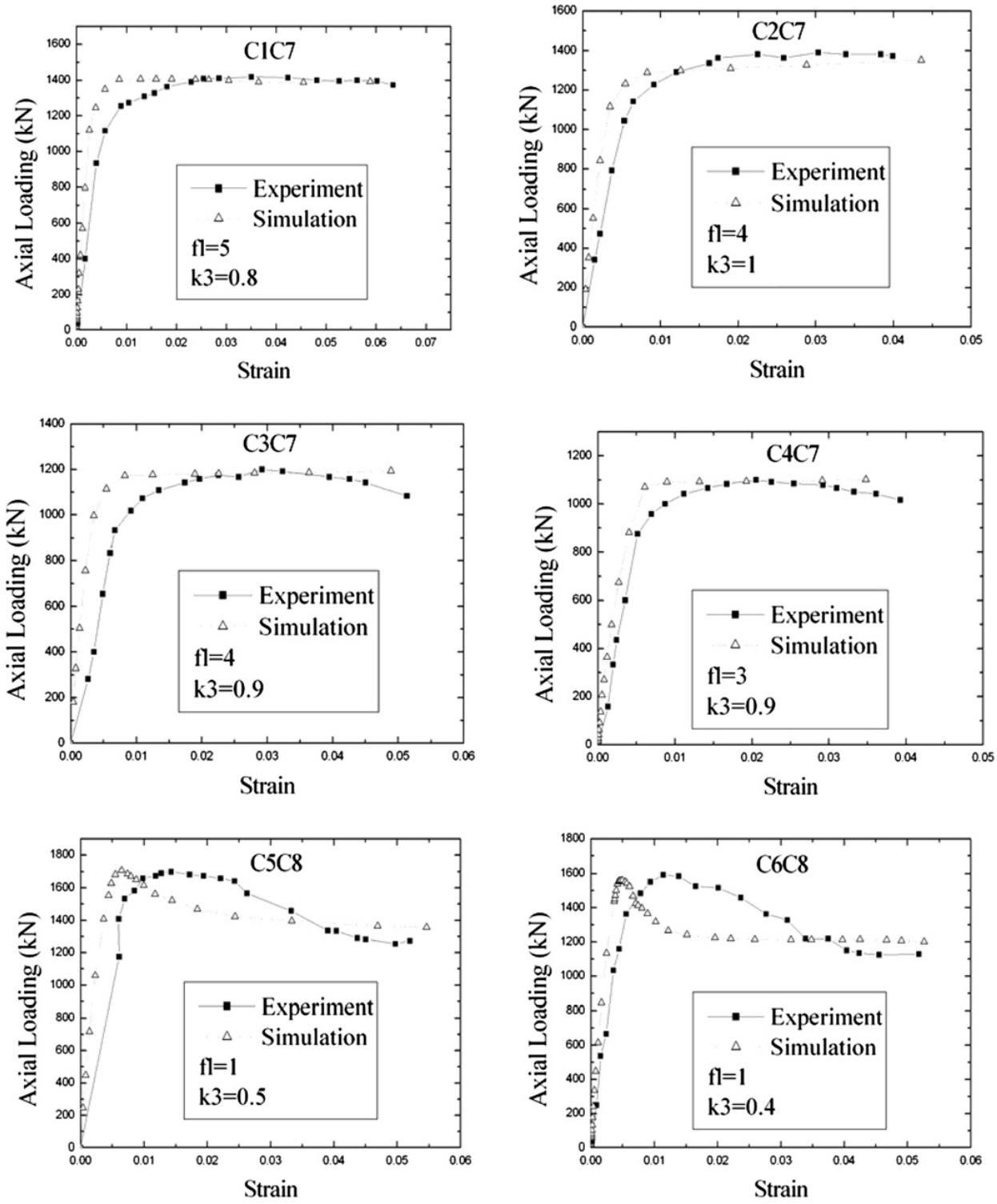

Fig. 7. Axial loading–strain relations of the CFDST columns tested by Zhao et al.

Regression analyses of the multivariate statistics method [28,29] are applied to the numerical results of CFDST to fit a surface through the lateral confining pressure f_l. The following three equations are proposed for f_l:

$$f_l = a_1 + a_2(D_o/t_o) + a_3(D_i/t_i) + a_4(D_o/t_o)^2 + a_5(D_o/t_o)(D_i/t_i) + a_6(D_i/t_i)^2 \quad (8a)$$

Table 2
Results of numerical analyses.

Column number	Ultimate strength (kN)			Failure strength (kN)			$f_{l\,(\mathrm{MPa})}$	k_3
	Experiment	Analysis	Error (%)	Experiment	Analysis	Error (%)		
CC2a	1800	1870	3.89	1247	1205	3.34	4	0.3
CC3a	1665	1699	2.04	1185	1152	2.78	3	0.3
CC5a	915	910	0.55	885	860	2.82	5	0.6
CC6a	2430	2505	3.09	1620	1612	0.49	2	0.3
CC7a	3330	3327	0.09	2010	2150	1.99	1	0.3
C1C7	1418	1407	0.77	1372	1391	1.38	5	0.8
C2C7	1390	1352	2.73	1372	1352	1.46	4	1
C3C7	1191	1193	0.17	1083	1193	0.92	4	0.9
C4C7	1100	1104	0.36	1016	1104	8.66	3	0.9
C5C8	1700	1707	0.41	1272	1355	6.53	1	0.5
C6C8	1591	1560	1.95	1127	1199	6.39	1	0.4

$$f_l = a_1 + a_2(D_o/t_o) + a_3(D_i/t_i) + a_4(D_o/t_o)(D_i/t_i) \tag{8b}$$

$$f_l = a_1 + a_2(D_o/t_o) + a_3(D_i/t_i) \tag{8c}$$

After the coefficients in Eq. (8) are obtained, the values of R^2 (coefficient of determination) [28,29] for these equations are calculated, which are equal to 0.8306, 0.7653 and 0.5967 for Eqs. (8a)–(8c), respectively. Since the value of R^2 for Eq. (8a) is the largest, Eq. (8a) is selected as the proposed equation for the lateral confining pressure f_l as follows:

$$f_l = 8.525 - 0.166(D_o/t_o) - 0.00897(D_i/t_i) + 0.00125(D_o/t_o)^2 + 0.00246(D_o/t_o) \times (D_i/t_i) - 0.00550(D_i/t_i)^2 \geq 0 \tag{9}$$

Eq. (9) is plotted as a three-dimensional surface in Fig. 11a showing the values of f_l versus the ratios D_o/t_o and D_i/t_i for the CFDST columns in analyses. From Fig. 11b, we can observe that when the diameter-to-thickness ratio of the inner tube D_i/t_i is equal to 15, 25 or 35, the lateral confining pressure

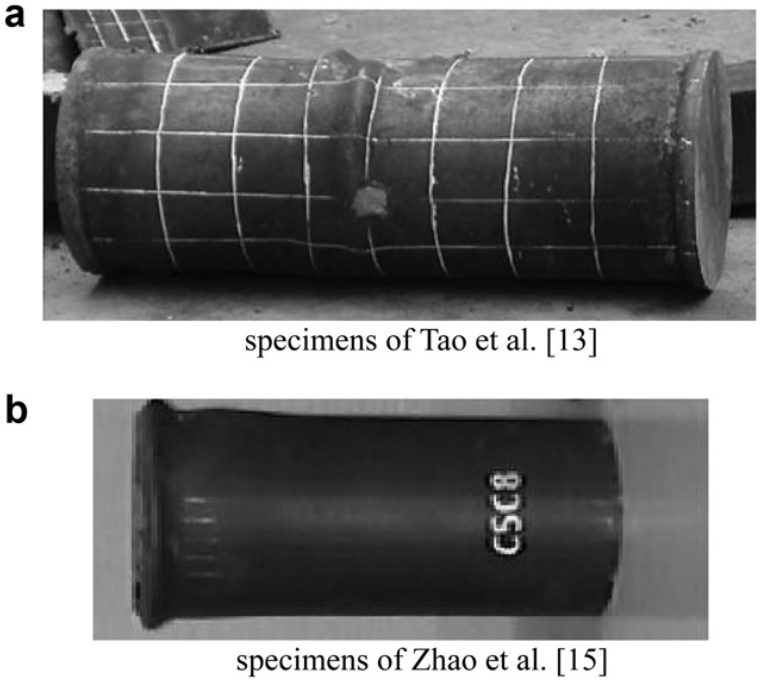

Fig. 8. Typical failure patterns of the CFDST columns in experiments.

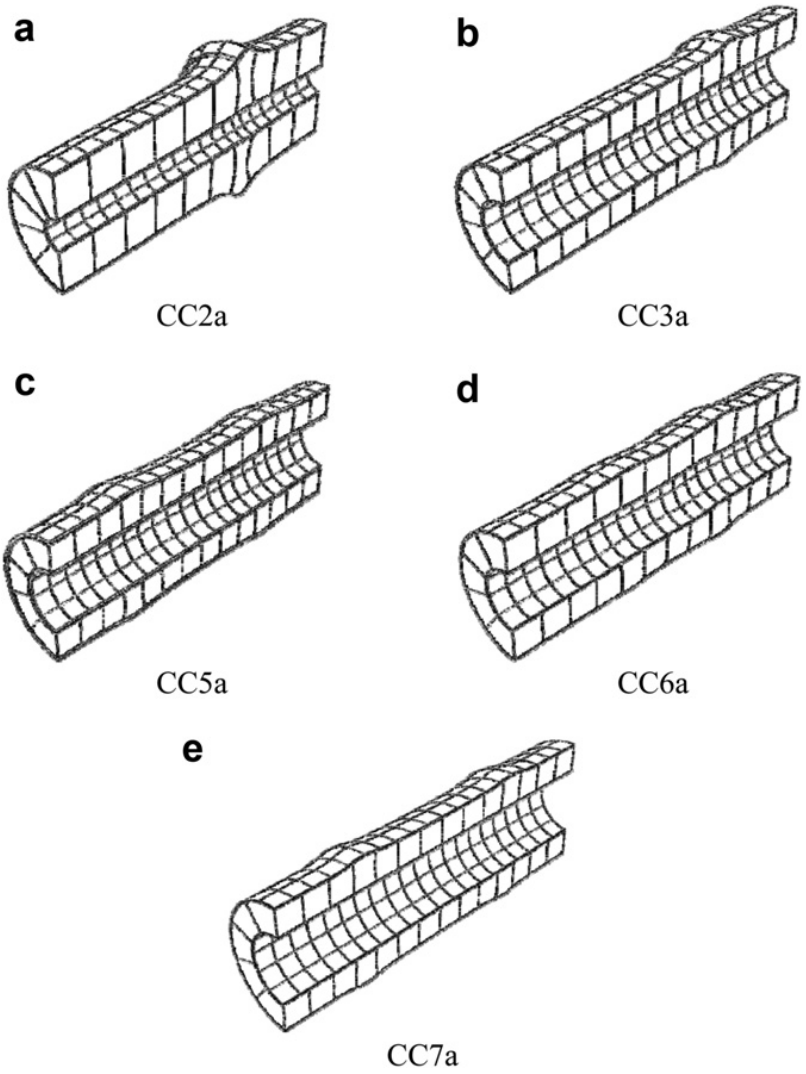

Fig. 9. Deformation shapes of the simulated CFDST columns tested by Tao et al.

f_l initially decreases with the increasing of the D_o/t_o ratio. However, after the minimum value of f_l is reached, the lateral confining pressure starts to increase with the increasing of the D_o/t_o ratio. For example, columns C1C7, C2C7, C3C7 and C4C7 have the same $D_i/t_i = 17.29$ ratio. The minimum value of f_l may be reached when D_o/t_o ratio is around 50. Since the D_o/t_o ratios for these columns are smaller than 50, the lateral confining pressure f_l decreases with the increasing of the D_o/t_o ratio. If the D_o/t_o ratios for these columns are greater than 50, the lateral confining pressure will start to increase with the increasing of the D_o/t_o ratio. When the diameter-to-thickness ratio of the inner tube D_i/t_i is equal to 45 or 55, the lateral confining pressure f_l is usually zero. However, after certain D_o/t_o ratio is reached, the lateral confining pressure starts to increase with the increasing of the D_o/t_o ratio.

From Fig. 11c, we can observe that when the diameter-to-thickness ratio of the outer tube D_o/t_o is equal to 40 or 80, the lateral confining pressure f_l usually decreases with the increasing of the D_i/t_i ratio. When the diameter-to-thickness ratio of the outer tube D_o/t_o is equal to 100, the lateral confining pressure f_l initially increases with the increasing of the D_i/t_i ratio. However, after the maximum value of f_l is reached, the lateral confining pressure starts to decrease with the increasing of the D_i/t_i ratio.

4.3. *Parameter study for* f_l/f_{yi}

In this section, the lateral confining pressure f_l is normalized by the yield strength of the inner tube, f_{yi}. Similar regression analyses as those in the previous section are applied to the numerical results of

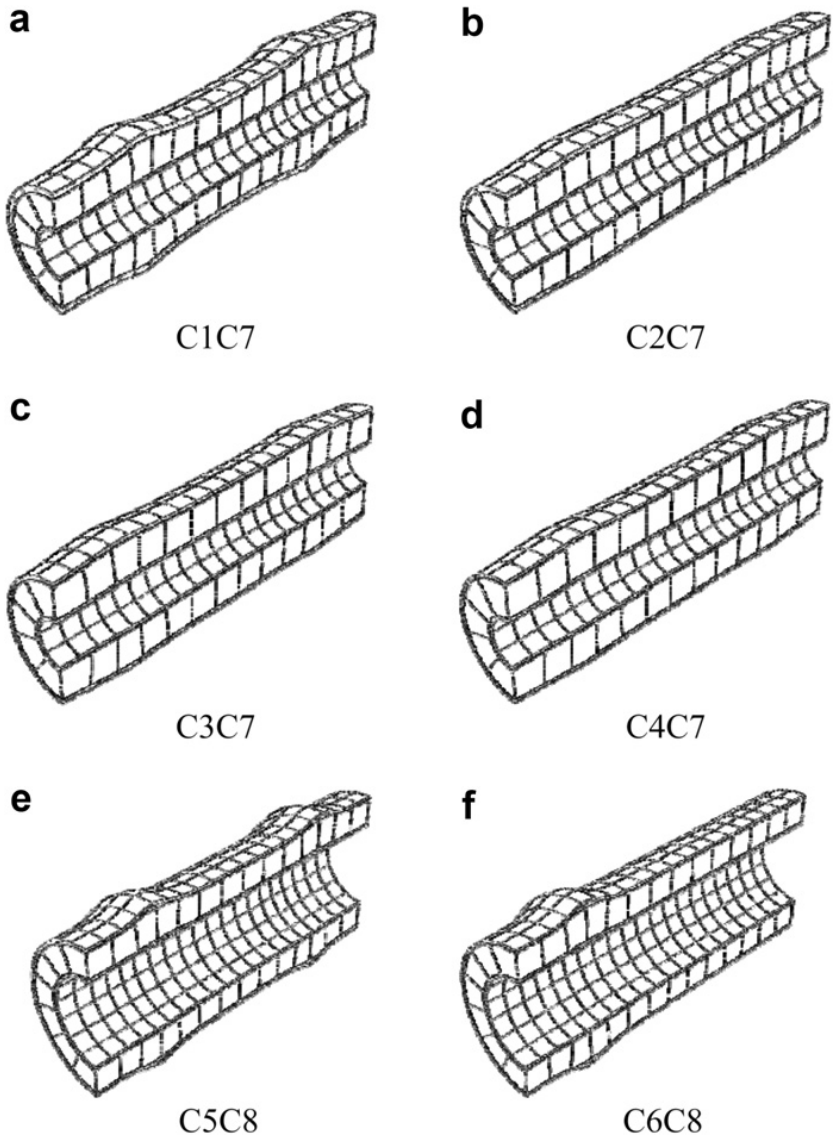

Fig. 10. Deformation shapes of the simulated CFDST columns tested by Zhao et al.

CFDST to fit a surface through the normalized value of f_l/f_{yi}. The values of R^2 for Eqs. (8a)–(8c) with f_l replaced by f_l/f_{yi} are 0.6985, 0.5677 and 0.4501, respectively. Since the largest value of R^2 is 0.6985, the proposed equation for the normalized value of f_l/f_{yi} is given as follows:

$$f_l/f_{yi} = 0.01844 - 0.00055(D_o/t_o) + 0.00040(D_i/t_i) + 0.00001(D_o/t_o)^2 + 0.00001(D_o/t_o) \times (D_i/t_i) - 0.00002(D_i/t_i)^2 \quad (10)$$

Fig. 12 shows the values of f_l/f_{yi} versus D_o/t_o and D_i/t_i for the CFDST columns in analyses. It can be seen that it shows the similar trend as that in Fig. 11.

4.4. Parameter study for f_l/f_{yo}

In this section, the lateral confining pressure f_l is normalized by the yield strength of the outer tube, f_{yo}. Similar regression analyses as those in the previous sections are applied to the numerical results of CFDST to fit a surface through the normalized value of f_l/f_{yo}. The values of R^2 for Eqs. (8a)–(8c) with f_l

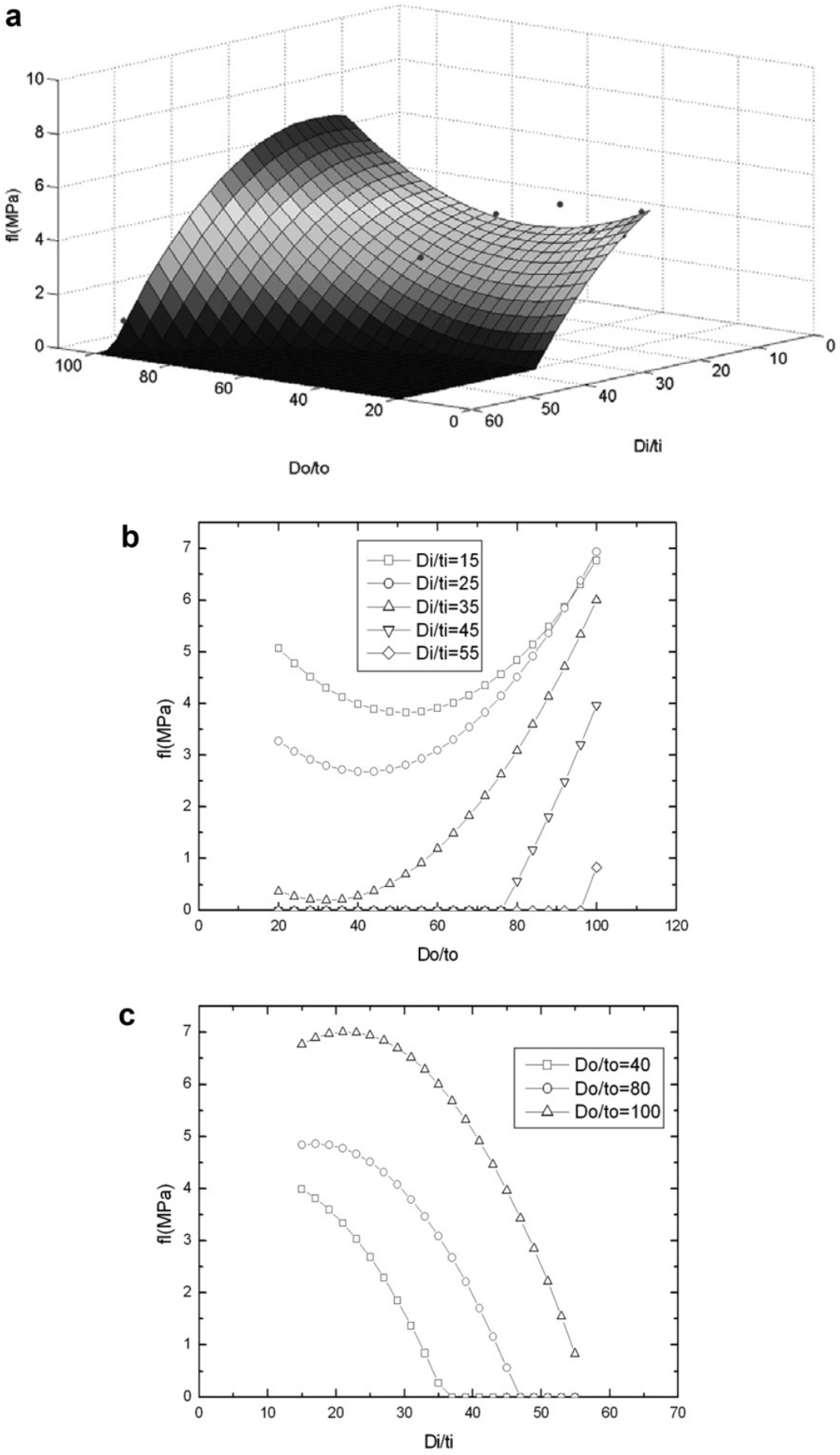

Fig. 11. f_l versus D_o/t_o and D_i/t_i for CFDST columns.

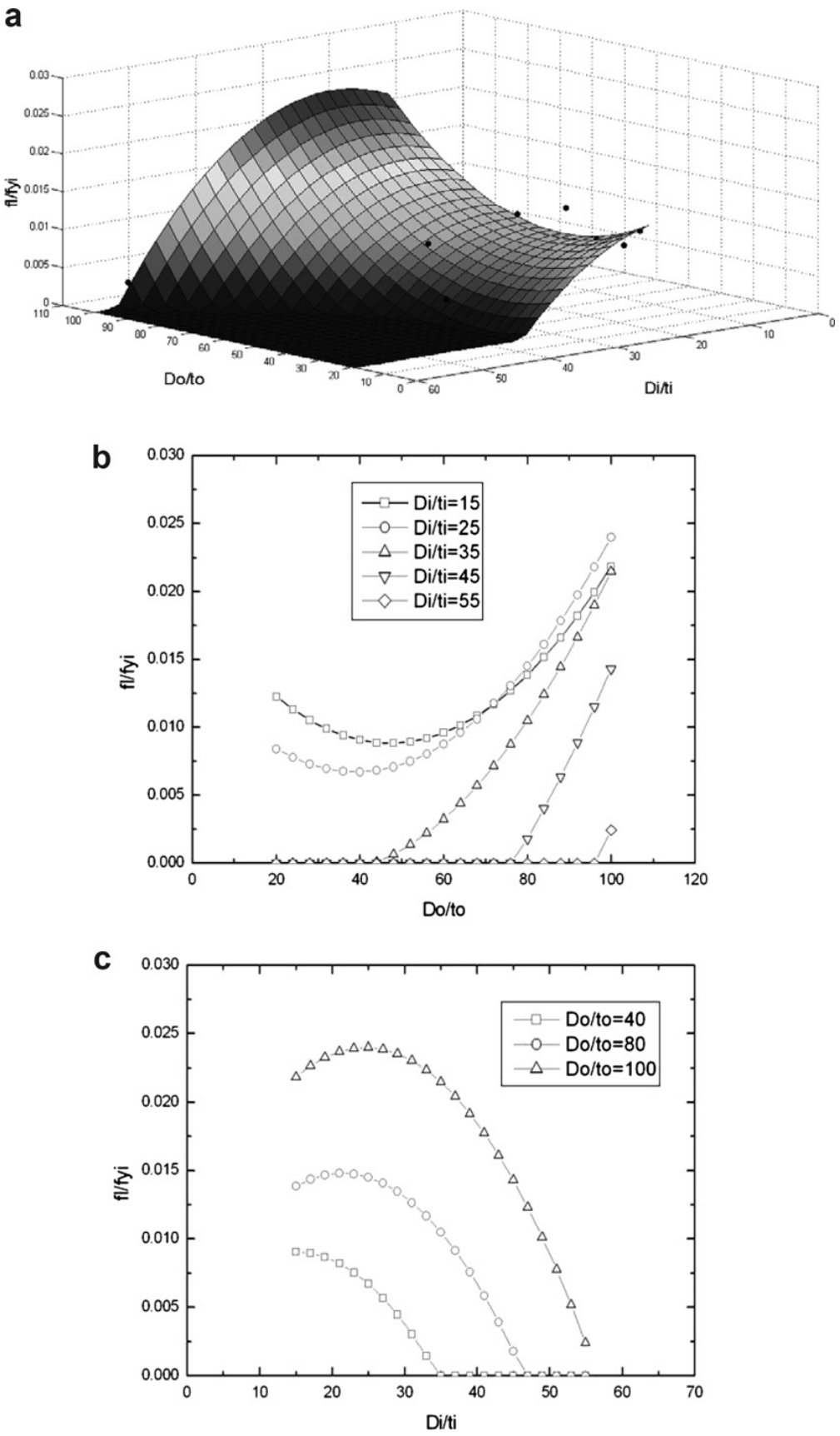

Fig. 12. f_l/f_{yi} versus D_o/t_o and D_i/t_i for CFDST columns.

replaced by f_l/f_{yo} are 0.5397, 0.4702 and 0.4332, respectively. Since the largest value of R^2 is 0.5397, the proposed equation for the normalized value of f_l/f_{yo} is given as follows:

$$f_l/f_{yo} = 0.01791 - 0.00036(D_o/t_o) - 0.00013(D_i/t_i) + 0.00001(D_o/t_o)^2 + 0.00001(D_o/t_o) \times (D_i/t_i) - 0.00002(D_i/t_i)^2 \geq 0 \tag{11}$$

Fig. 13 shows the values of f_l/f_{yo} versus D_o/t_o and D_i/t_i for the CFDST columns in analyses and it exhibits the similar trend as that in Fig. 11.

In this paper, three equations, i.e. Eqs. (9)–(11), are proposed to predict the lateral confining pressure f_l for the CFDST columns. For practical engineering application, the minimum value of f_l predicted by these three equations could be used.

4.5. Parameter study for k_3

The material degradation parameter k_3 is used to model the behavior of concrete beyond the ultimate strength. It should be noted that the value of k_3 varies between 0 and 1. Similar regression analyses as those in the previous sections are applied to the numerical results of CFDST to fit a surface through the value of k_3. The values of R^2 for Eqs. (8a)–(8c) with f_l replaced by k_3 are 0.8961, 0.8562 and 0.7200, respectively. Since the largest value of R^2 is 0.8961, the proposed equation for the material degradation parameter k_3 is given as follows:

$$k_3 = 1.73916 - 0.00862(D_o/t_o) - 0.04731(D_i/t_i) - 0.00036(D_o/t_o)^2 + 0.00134(D_o/t_o)(D_i/t_i) - 0.00058(D_i/t_i)^2 \geq 0 \tag{12}$$

Fig. 14 shows the values of k_3 versus D_o/t_o and D_i/t_i for the CFDST columns. It can be observed that the surface of k_3 has a saddle shape (Fig. 14a). When the D_o/t_o and the D_i/t_i ratios are small, the material degradation parameter k_3 usually has a large value.

5. Comparison between the proposed design formulations with the AISC formulations

In this section, the relevant design formulations according to AISC specification [30] are modified slightly. The calculated axial ultimate strengths of CFDST columns based on the AISC formulations and the proposed formulations are compared to the experimental data.

According to the AISC specification [30], the axial ultimate strength P_n of CFDST column can be obtained using the following expressions:

$$P_n = P_o\left[0.658^{(P_o/P_e)}\right] \quad when \quad P_e \geq 0.44P_o \tag{13a}$$

$$P_n = 0.877P_e, \ when \ P_e < 0.44P_o \tag{13b}$$

where

$$P_o = A_s f_y + C_2 A_c f_c' \tag{14}$$

$$C_2 = 0.85 \ for \ rectangular \ cross \ sections \tag{15a}$$

$$C_2 = 0.95 \ for \ circular \ cross \ sections \tag{15b}$$

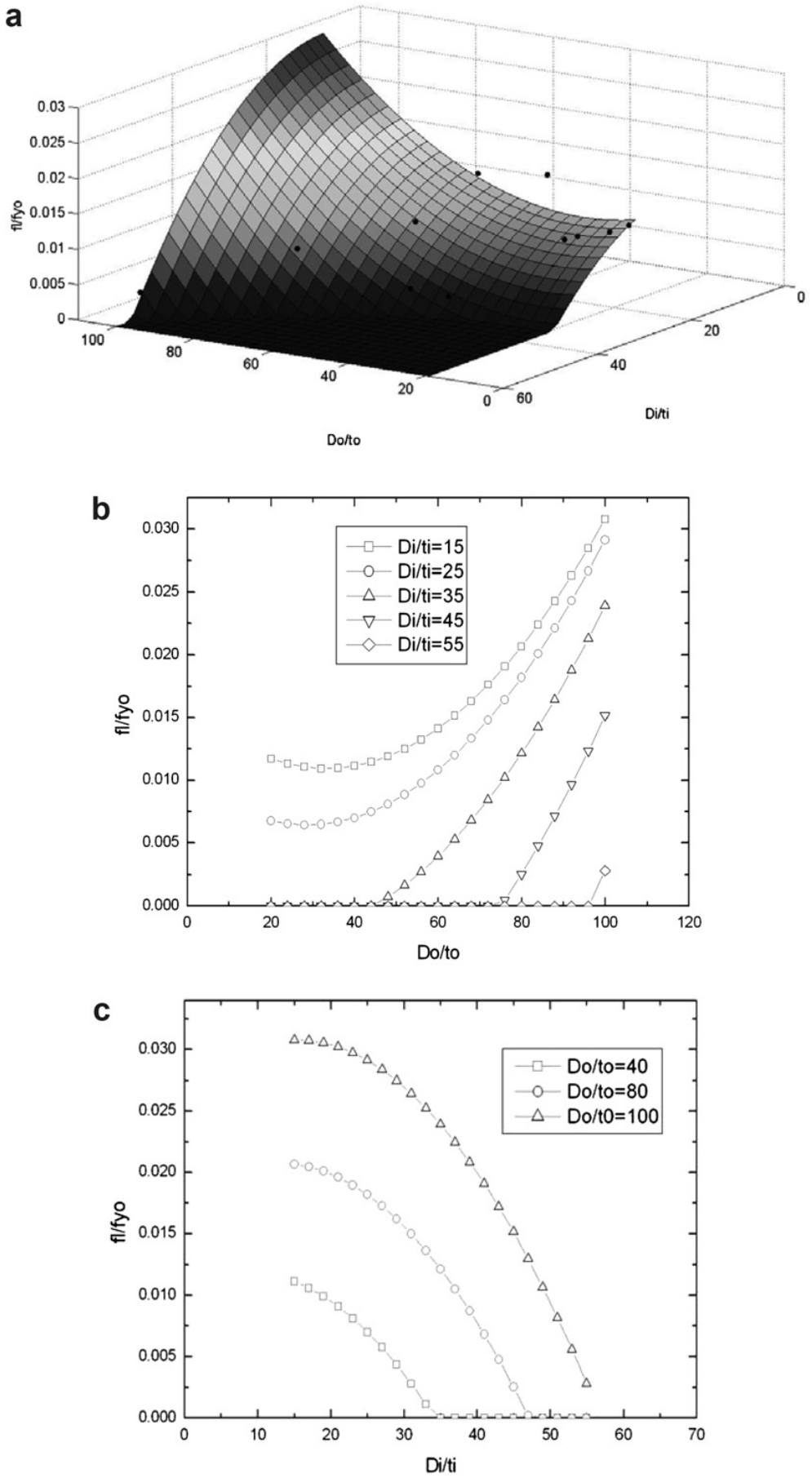

Fig. 13. f_l/f_{yo} versus D_o/t_o and D_i/t_i for CFDST columns.

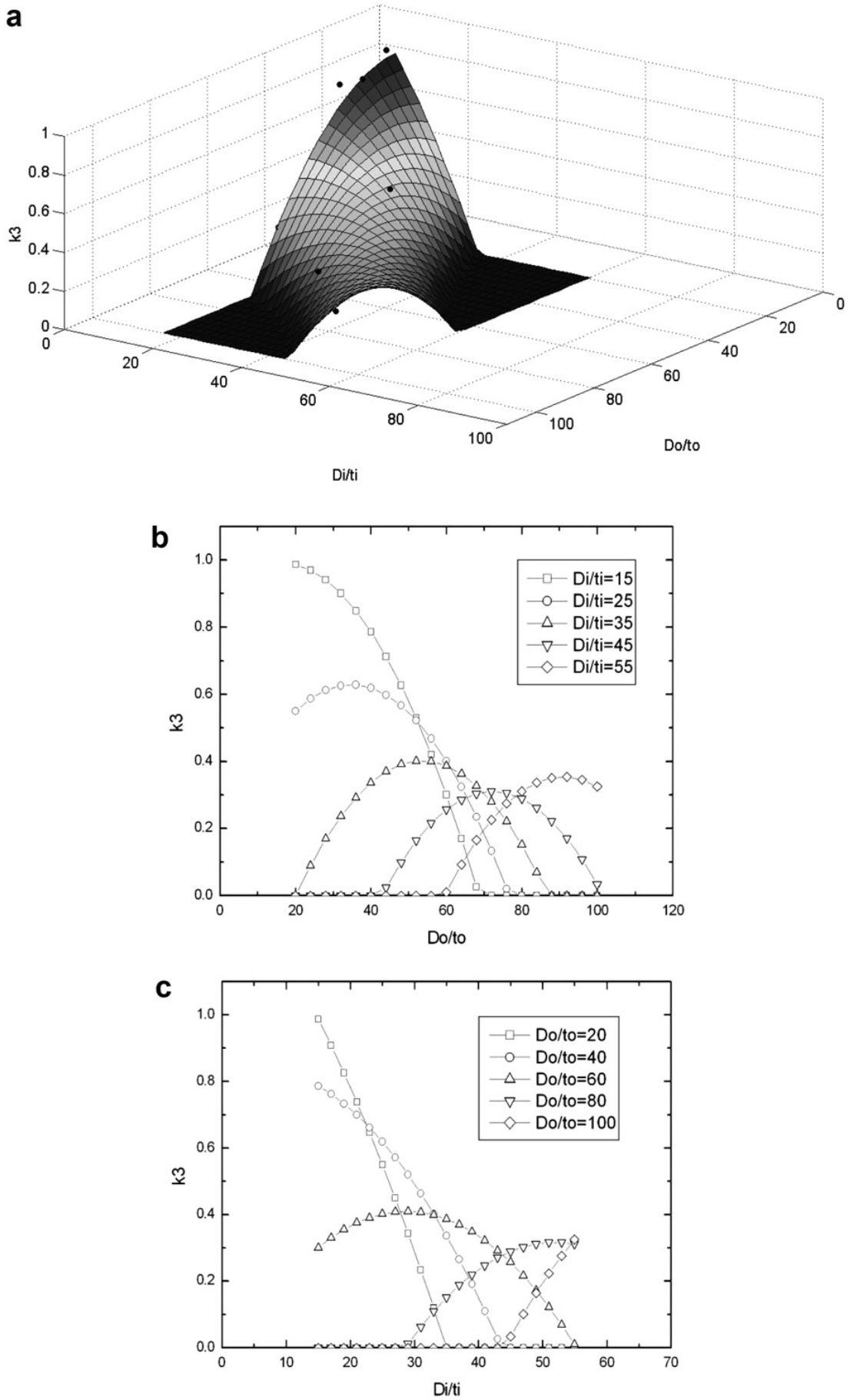

Fig. 14. k_3 versus D_o/t_o and D_i/t_i for CFDST columns.

$$P_e = \frac{\pi^2}{(KL)^2}(E_s I_s + C_3 E_c I_c) \tag{16}$$

$$C_3 = 0.6 + 2\left(\frac{A_s}{A_s + A_c}\right) \leq 0.9 \tag{17}$$

In the above equations, A_s and A_c are the cross-section areas of steel tubes and concrete, respectively. L is the laterally unbraced length of the CFDST column. The constant K is the effective length factor and is equal to 2 for the CFDST columns in this investigation. I_s and I_c are the moments of inertia of steel tubes and concrete, respectively. The values of A_s, A_c, I_s and I_c can be calculated using the following expressions.

$$A_s = \frac{\pi}{4}\left[D_o^2 - (D_o - 2t_o)^2 + D_i^2 - (D_i - 2t_i)^2\right] \tag{18a}$$

$$A_c = \frac{\pi}{4}\left[(D_o - 2t_o)^2 - D_i^2\right] \tag{18b}$$

$$I_s = \frac{\pi}{64}\left[D_o^4 - (D_o - 2t_o)^4 + D_i^4 - (D_i - 2t_i)^4\right] \tag{19a}$$

$$I_c = \frac{\pi}{64}\left[(D_o - 2t_o)^4 - D_i^4\right] \tag{19b}$$

In Eq. (16), the modulus of elasticity of steel E_s is equal to 200 GPa for the CFDST columns in this investigation. The modulus of elasticity of concrete E_c can be calculated as [25]

$$E_c = 0.043 w_c^{1.5} \sqrt{f_c'}\, MPa \tag{20}$$

where w_c is the density of concrete. For normal-weight concrete, it may be assumed that $w_c = 2400$ kg/m^3.

For the formulations proposed by the authors to calculate the ultimate strengths of the CFDST columns, only Eqs. (14) and (20) are slightly modified by replacing the compressive strength of concrete f_c' with the confined compressive strength of concrete f_{cc}'. The rest formulations are the same as those in AISC specification. The two modified Eqs. become

$$P_o = A_s f_y + C_2 A_c f_{cc}' \tag{21}$$

$$E_c = 0.043 w_c^{1.5} \sqrt{f_{cc}'}\, MPa \tag{22}$$

The value of f_{cc}' can be obtained from Eq. (2), which is listed below.

$$f_{cc}' = f_c' + k_1 f_l$$

In the above expression, k_1 is equal to 4.1 and the value of the lateral confining pressure f_l is the minimum value obtained by Eqs. (9)–(11). Table 3 shows the parameters used to calculate the ultimate strengths of the CFDST columns. Table 4 shows the ultimate strengths of the CFDST columns calculated by the AISC formulations and the proposed formulations. It can be observed that the proposed formulations are better than the AISC formulations. For some specimens (say CC2a and CC6a), the error percentages are reduced significantly.

Table 3
Parameters for calculating the ultimate strengths of CFDST columns.

Column number	C_3	f_l (MPa)	f_c' (MPa)	f_{cc}' (MPa)	E_c (MPa)		P_e (kN)		$0.44P_o$ (kN)	
					$0.043w_c^{1.5}\sqrt{f_c'}$	$0.043w_c^{1.5}\sqrt{f_{cc}'}$	AISC	Proposed	AISC	Proposed
CC2a	0.77	3.8	40	55.8	31,975	37,758	9379	11,073	621	766
CC3a	0.84	2.3	40	49.3	31,975	35,516	9626	10,690	596	665
CC5a	0.99	2.8	40	51.6	31,975	36,325	3725	4231	311	343
CC6a	0.78	2.0	40	48.2	31,975	35,100	16,543	18,157	947	1059
CC7a	0.77	0.8	40	43.2	31,975	33,224	24,807	25,774	1303	1365
C1C7	1.15	5.0	63.4	83.8	40,256	46,287	2910	3345	622	677
C2C7	1.06	4.0	63.4	79.8	40,256	45,163	3217	3608	552	599
C3C7	0.97	4.0	63.4	79.8	40,256	45,163	3505	3931	494	544
C4C7	0.93	3.0	63.4	75.7	40,256	43,988	3614	3949	466	504
C5C8	0.98	1.0	63.4	67.3	40,256	41,475	14,212	14,642	799	817
C6C8	0.94	1.0	63.4	67.5	40,256	41,537	14,824	15,296	738	758

Table 4
Ultimate strengths of CFDST columns calculated by the AISC formulations and the proposed formulations.

Column number	Ultimate strength (kN)			Error (%)	
	Experiment	AISC	Proposed	AISC	Proposed
CC2a	1800	1334	1641	−25.89	−8.85
CC3a	1665	1284	1432	−22.91	−13.98
CC5a	915	659	727	−28.02	−20.53
CC6a	2430	2048	2289	−15.72	−5.80
CC7a	3330	2830	2963	−15.02	−11.01
C1C7	1418	1177	1293	−17.02	−8.80
C2C7	1390	1083	1180	−22.12	−15.09
C3C7	1191	995	1097	−16.44	−7.86
C4C7	1100	948	1026	−13.84	−6.74
C5C8	1700	1729	1770	1.72	4.14
C6C8	1591	1607	1652	1.01	3.80

6. Conclusion

In this paper, nonlinear finite element analysis was conducted for CFDST columns. Based on the numerical results, the following conclusions were obtained:

(1) When the diameter-to-thickness ratio of the outer tube D_o/t_o is held constant, both the ultimate strength and the lateral confining pressure f_l decrease with the increasing of the diameter-to-thickness ratio of the inner tube D_i/t_i. Similarly, when the diameter-to-thickness ratio of the inner tube D_i/t_i is held constant, both the ultimate strength and the lateral confining pressure f_l also decreases with the increasing of the diameter-to-thickness ratio of the outer tube D_o/t_o.
(2) Double skin concrete-filled tubes can provide a good confining effect for concrete, especially when the diameter-to-thickness ratios of the outer and inner tubes (D_o/t_o, D_i/t_i) are small.
(3) For practical engineering application, the minimum value of f_l predicted by equations (9)–(11) could be used.
(4) When the D_o/t_o and the D_i/t_i ratios are small, the material degradation parameter k_3 usually has a large value. The value of k_3 might be predicted by Eq. (12).
(5) Based on the experiment data, the proposed design equations are applicable to the CFDST columns with the diameter to thickness ratios fallen in the ranges $20 \le D_o/t_o \le 100$ and $16 \le D_i/t_i \le 55$. Such ranges of diameter to thickness ratios are ordinary for engineering applications.
(6) The comparison of the proposed formulations with the AISC formulations against the experimental data shows that the proposed formulations are better than the AISC formulations. For some specimens (say CC2a and CC6a), the error percentages are reduced significantly.

References

[1] Ge HB, Usami T. Strength of concrete-filled thin-walled steel box columns: experiment. Journal of Structural Engineering, ASCE 1992;118(1):3036–54.
[2] Boyd FP, Cofer WF, McLean D. Seismic performance of steel-encased concrete column under flexural loading. ACI Structural Journal 1995;92(3):355–65.
[3] Bradford MA. Design strength of slender concrete-filled rectangular steel tubes. ACI Structural Journal 1996;93(2):229–35.
[4] Schneider SP. Axial loaded concrete-filled steel tubes. Journal of Structural Engineering, ASCE 1998;124(10):1125–38.
[5] Roeder CW, Cameron B, Brown CB. Composite action in concrete filled tubes. Journal of Structural Engineering, ASCE 1999; 125(5):477–84.
[6] Huang C-S, Yeh Y-K, Liu G-Y, Hu H-T, Tsai KC, Weng YT, et al. Axial load behavior of stiffened concrete-filled steel columns. Journal of Structural Engineering, ASCE 2002;128(9):1222–30.
[7] Elchalakani M, Zhao XL, Grzebieta RH. Plastic mechanism analysis of circular tubes under pure bending. International Journal of Mechanical Sciences 2002;44(6):1117–43.
[8] Hu H-T, Huang CS, Wu M-H, Wu Y-M. Nonlinear analysis of axially loaded CFT columns with confinement effect. Journal of Structural Engineering, ASCE 2003;129(10):1322–9.
[9] Hu H-T, Huang CS, Chen ZL. Finite element analysis of CFT columns subjected to combined axial force and bending moment. Journal of Constructional Steel Research 2005;61(12):1692–712.
[10] Lu FW, Li SP, Sun G. A study on the behavior of eccentrically compressed square concrete-filled steel tube columns. Journal of Constructional Steel Research 2007;63(7):941–8.
[11] Lin ML, Tsai KC. Behavior of double-skinned composite steel tubular columns subjected to combined axial and flexural loads. In: Proceedings of the first international conference on steel and composite structures, Pusan, Korea, June 14–16, 2001, pp. 1145–52.
[12] Han L-H, Huang H, Tao Z, Zhao XL. Concrete-filled double skin steel tubular (CFDST) columns subjected to cyclic bending. Engineering Structures 2006;29(12):1698–714.
[13] Tao Z, Han LH, Zhao XL. Behaviour of concrete-filled double skin (CHS inner and CHS outer) steel tubular stub columns and beam-columns. Journal of Constructional Steel Research 2004;60(8):1129–58.
[14] Wei S, Mau ST, Vipulanandan C, Mantrala SK. Performance of new sandwich tube under axial loading: experiment. Journal of Structural Engineering, ASCE 1995;121(12):1806–14.
[15] Zhao XL, Grzebieta RH, Elchalakani M. Tests of concrete-filled double skin CHS composite stub columns. Steel and Composite Structures 2002;2(2):129–46.
[16] Han LH, Xu L, Zhao XL. Tests and analysis on the temperature field within concrete-filled steel tubes with or without protection subjected to a standard fire. Advances in Structural Engineering 2003;6(2):121–33.
[17] Dawson TH. Offshore structural engineering. Prentice-Hall Inc.; 1983.
[18] Sumer BM, Fredsoe J. Hydrodynamics around cylindrical structures. World Scientific; 1997.
[19] Abaqus. Analysis user's manuals and example problems manuals, version 6.9. Providence, Rhode Island: Abaqus, Inc.; 2009.
[20] ASCE Task Committee on Concrete and Masonry Structure. State of the art report on finite element analysis of reinforced concrete. New York: ASCE; 1982.
[21] Mander JB, Priestley MJN, Park R. Theoretical stress-strain model for confined concrete. Journal of Structural Engineering, ASCE 1988;114(8):1804–23.
[22] Richart FE, Brandtzaeg A, Brown RL. A study of the Failure of Concrete under Combined Compressive Stresses Bulletin, vol. 185. Champaign, Illinois: University of Illinois Engineering Experimental Station; 1928.
[23] Saenz LP. Discussion of "Equation for the stress-strain curve of concrete" by Desayi P, Krishnan S. ACI Journal 1964;61: 1229–35.
[24] Hu HT, Schnobrich WC. Constitutive modelling of concrete by using nonassociated plasticity. Journal of Materials in Civil Engineering, ASCE 1989;1(4):199–216.
[25] ACI Committee 318. Building code requirements for structural concrete and commentary (ACI 318-08). Detroit, Michigan: American Concrete Institute; 2008.
[26] Uy B. Local and post-local buckling of concrete filled steel welded box columns. Journal of Constructional Steel Research 1998;47(1–2):47–72.
[27] Zhao XL, Grzebieta RH. Strength and ductility of concrete filled double skin (SHS inner and SHS outer) tubes. Thin-Walled Structures 2002;40(2):199–213.
[28] Lancaster P, Salkauskas K. Curve and surface fitting: an introduction. Academic Press; 1986.
[29] Tabachnick BG, Fidell LS. Using multivariate statistics. 5th ed. Allyn and Bacon; 2006.
[30] AISC Committee on Specifications. Specification for structural steel buildings, ANSI/AISC 360-05. Chicago: American Institute of Steel Construction; 2005.